Recoil ion charge state distribution following the β^+ decay of ^{21}Na

N. D. Scielzo, S. J. Freedman, B. K. Fujikawa, and P. A. Vetter
Department of Physics, University of California at Berkeley and
Lawrence Berkeley National Laboratory, Berkeley, California 94720
(Dated: December 23, 2002)

The charge state distribution following the β^+ decay of ^{21}Na has been measured, with a larger than expected fraction of the daughter ^{21}Ne in positive charge states. No dependence on either the β^+ or recoil nucleus energy is observed. The data is compared to a simple model based on the sudden approximation. Calculations suggest a small but important contribution from recoil ionization has important consequences for precision β decay correlation experiments detecting recoil ions.

I. INTRODUCTION

Measurements of recoil ion spectra in nuclear β decay are useful probes of the Weak Interaction. The energy spectra of ^{6}He[1–3], ^{23}Ne[1, 4], ^{19}Ne[1, 5], and ^{35}Ar[1] decays led to the discovery of the $V-A$ (vector minus axial vector) structure and the ^{6}He $\beta-\nu$ correlation[3] provides the best limit to a possible tensor component. The recoil ion spectrum from the electron capture (EC) decay of ^{37}Ar recently put limits on the admixture of heavy neutrinos[6, 7].

Trapped radioactive atoms and ions are appealing sources of activity for a new generation of precise β decay experiments testing the Standard Model. Radioactive nuclei are confined to a small volume ($\sim$1 mm^3), decay essentially at rest (velocities $\lesssim$1 m/s), and the recoil daughters emerge with minimal perturbation. Daughter ions can be manipulated with electric and magnetic fields. Several β decay correlation measurements are currently underway[8, 9] or nearing an interesting precision of $\sim$0.01[10], and further improvements are expected.

In interpreting recoil ion measurements, the charge state production is assumed to be independent of the β and nuclear recoil energy. For β^+ emitters, ionization mechanisms are critical since positively charged daughter ions are formed only when $\geq$2 orbital electrons are lost. Negative ions, if formed at all, are often unstable and of limited utility for measurements. Ionization affects the statistical precision and can lead to systematic errors if dependent on β or recoil ion energy. For example, ionization dependent on nuclear momentum would alter each charge state's recoil energy spectrum, leading to an experiemental signature similar to a $\beta-\nu$ correlation.

Understanding the ionization state following β decay is interesting in its own right. Charge state distributions have been measured in a number of noble gas atoms. For β^- emitters, such as ^{6}He[11], ^{23}Ne[12], ^{85}Kr[13], and ^{41}Ar[14], electron shake-off (SO) resulting from parent/daughter orbital mismatch is the dominant process. The charge state distribution decreases with increasing charge, with 80–90% of daughter ions having a charge +1 and $<$5% with charge $\geq$3. In addition, inner shell vacancies lead to dramatic ionization from Auger cascades in the electron capture (EC) decay of ^{37}Ar[15, 16], the internal conversion (IC) of ^{131m}Xe[17], and the β^- and IC decay of ^{133}Xe[18].

Until recent experiments with radioactive trapped atoms, there was no data on charge state production following β^+ emission. Although ^{79}Kr decays by both β^+ emission and EC and has been demonstrated to produce positive ions, neutrals, and negative ions[19], the decay is predominantly EC. A simple estimate equating the net electron loss in β^- and β^+ decay indicates $<$5% of the daughters should be in positive charge states, with yield decreasing with increasing ion charge state.

Laser trapped ^{38m}K[10] and the present ^{21}Na results show this greatly underestimates the production of positive daughter ions for these β^+ emitters. We measure the charge state distribution by detecting the β^+ and recoil ion in coincidence. The β energy dependence of ion production allows us to check the independence of the ionization process from the decay product energies.

Nuclear recoil can have a large ionizing effect for high energy γ-ray[20], nucleon[20], and α emission[21]. In β decay, recoil ionization is usually assumed to be small in all atoms studied except ^{6}He where the large endpoint energy, E_0, and small nuclear mass leads to recoil energies of up to 1400 eV. Nuclear recoil contributes 3% to the production of ^{6}Li^{+2}, and $>$50% to the production of ^{6}Li^{+3}[11]. No evidence of recoil ionization was found in a similar study of charge states +2 through +5 of ^{23}Ne β^- decay, although the limit is not particularly restrictive[12].

Ionization in the K shell can have significant β energy dependence, as in the β^- decays of ^{99}Tc[22] and ^{147}Pm[22, 23] where the binding energy, B_K, and E_0 are comparable. The direct collision (DC) mechanism, in which ionization results from the β knocking out an orbital electron, is also expected to be important for decays with comparable B_K and E_0. Detailed calculations indicate the DC mechanism can contribute significantly to ionization, even for decays with small B_K/E_0, and observed ionization disagrees with calculation unless a large DC contribution is included.

II. TRAPPING APPARATUS

The production and accumulation of ^{21}Na in a magneto-optical trap (MOT) has been described

elsewhere[24, 25] and will only be briefly summarized here. The ^{21}Na is produced through ^{24}Mg(p,α)^{21}Na by bombarding a powdered MgO target with 2μA of 25 MeV protons from the 88-Inch Cyclotron at Lawrence Berkeley National Laboratory. The alumina crucible containing the target is heated to $\sim$1000° C and the sodium diffuses out of the target at a rate of $\sim 3\times10^8$ atoms/sec. The atomic beam emerges through four narrow, alumina collimator tubes aimed at the trapping chamber. A two-dimensional optical molasses generated by 1 cm laser beams reflected four times across the atomic beam provides additional collimation 10 cm downstream from the beam nozzles.

Two Coherent 899 ring dye lasers using Rhodamine 6G dye generate laser light at 589 nm. The lasers are frequency stabilized using saturated absorption spectroscopy on the D_2 transition in ^{23}Na after passing through an acousto-optic modulator to account for the 1648 MHz isotope shift. An electro-optic modulator shifts $\sim$10% of the laser power to the $3^2S_{1/2}(F = 1)$ to $3^2P_{3/2}(F = 2)$ transition as a repump frequency to avoid optical pumping to the untrapped $3^2S_{1/2}(F = 1)$ hyperfine level.

A 8 mW/cm^2 slowdown laser beam detuned -20 MHz from the D_2 transition decelerates the atomic beam as it traverses a 1.2 m long "Zeeman-slower" solenoid. At the exit of the solenoid, an extraction coil provides a large, nearly constant magnetic field that decouples the atoms' velocity from resonance with the slowdown laser at a nonzero velocity. A 4 mm diameter "dark spot" in the center of the slowdown laser beam creates a shadow over the trap. Keeping the unbalanced force of the slowdown laser beam from destabilizing the trap doubles the number of atoms trapped.

The slow ^{21}Na atoms are captured in a 6 beam MOT. The trapping laser beams are 3.5 cm in diameter, have a detuning of 15 MHz, and each have an intensity of $\sim$6 mW/cm^2. Anti-Helmholtz coils surrounding the trap generate a quadrupole field with an axial gradient of 12 G/cm. Up to 8×10^5 ^{21}Na atoms have been trapped. The trap lifetime is 12$\pm$2 s. The trap is monitored by measuring fluorescence with a photomultiplier tube (PMT), and the trap position and spatial distribution is recorded with a CCD camera.

III. MEASUREMENT TECHNIQUE

The experimental arrangement is shown in Fig. 1. The trap is located between two detectors — a ΔE-E plastic scintillator telescope on one side, and a chevron microchannel plate (MCP) detector on the other. A system of stainless steel electrodes generates a static electric field of $\sim$1 kV/cm to guide positive ions from the trap to the MCP. A trigger in either portion of the β detector telescope opens a 3 μs coincidence window, providing time for the recoil ^{21}Ne to reach the MCP. For coincident events, we record the time between β detector (either

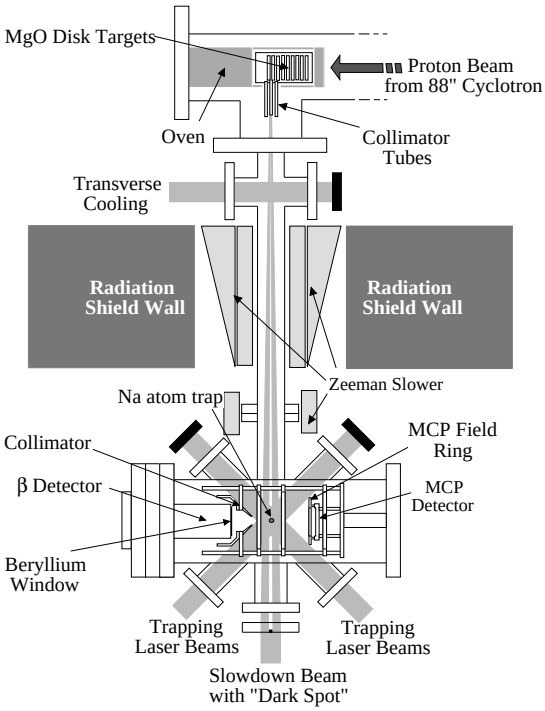

FIG. 1: Experimental arrangement shown is not drawn to scale. Anti-Helmholtz trapping coils (not shown) lay above and below the trapping chamber in the plane of the page.

ΔE or E) and MCP trigger, the pulse heights and singles rates from all three detectors, and the fluorescence signal from the trap measured with a PMT.

The ΔE and E scintillators are 1 mm and 15 mm thick respectively with diameters of 35.5 mm and 45 mm. Light from each scintillator is transported through light guides to separate, magnetic field insensitive PMTs (Hamamatsu R5924 for the ΔE scintillator and R5946 for the E scintillator). The ΔE and E components of the β detector are independently calibrated with radioactive sources. The total energy is determined from the sum of the deposited energies. The FWHM energy resolution of the β detector is 120$\pm$12 keV at the 364 keV ^{113}Sn conversion electron line and 150$\pm$15 keV at the 976 keV ^{207}Bi conversion electron line. The resolution is limited by the ΔE detector. At 92.5 mm from the trap, the β detector subtends 0.92% of 4π. We select events that trigger the ΔE and deposit >50 keV of energy in the β detector. Monte Carlo simulations that include energy loss in the 127 μm Be window that separates the β detector from the ultra-high vacuum indicate an effective energy cut at $\sim$175 keV and detection of 96.8$\pm$0.1% of the β spectrum.

A tungsten alloy collimator thick enough to stop βs of energies <3 MeV restricts the field of view of the β detector to a cone containing the trapped atoms. The collimator also prevents ions originating at the Be window from reaching the MCP. The electric field suppresses backgrounds by establishing a 2 kV potential barrier for

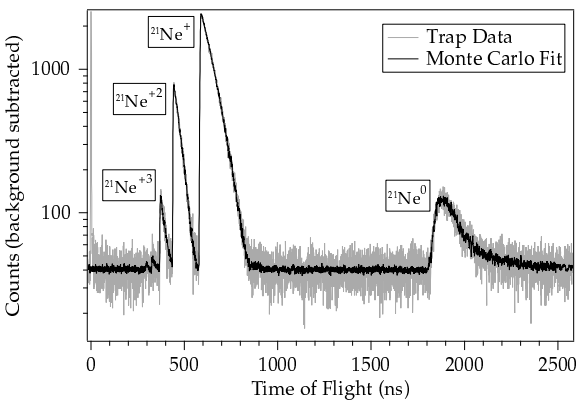

FIG. 2: Recoil ^{21}Ne time-of-flight spectrum. The inclusion of the experimental $\gamma-^{21}$Ne coincident TOF spectrum in the fit leads to the noise in the background level.

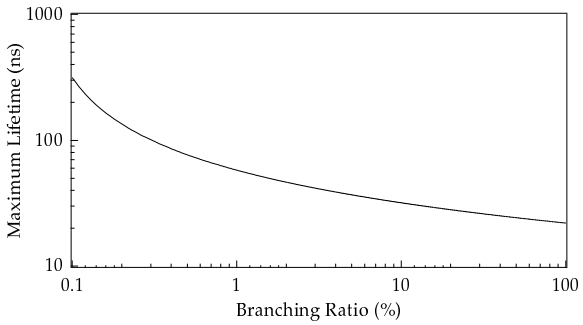

FIG. 3: Maximum lifetime of $^{21}Ne^{-}$ vs. its β decay branching ratio (68% C.L.), assuming the MCP detection efficiency decreases linearly at energies below 2 keV.

recoil ions originating on the chamber walls.

A Monte Carlo simulation generates the daughter ion's initial momentum distribution and the trajectories are calculated using the ion optics software package, SimIon 7.0. We use 5.02% for the branching ratio to the ^{21}Ne ($5/2^+$) excited state and the Standard Model values for both $\beta-\nu$ correlations. The Monte Carlo calculation predicts that >99.5% of $^{21}Ne^{+}$ and all higher ^{21}Ne charge states reach the MCP active area in coincidence with detected β^+s.

IV. EXPERIMENTAL RESULTS

The time-of-flight (TOF) recoil spectrum in Fig. 2 clearly reveals the ^{21}Ne charge states. Positive, negative, and neutral charge states are possible for β^+ decay. Our detector is far more sensitive to positive ions than neutral atoms, and it can only detect negative ions with electric fields reversed. As discussed below, we found no evidence of a negative ion state, and $^{21}Ne^{0}$, despite being the most prevalent, has the smallest absolute detection efficiency and largest uncertainties. With knowledge of the source activity and the detection efficiency for positive ion and β^+ coincidences, the entire charge state distribution can be reconstructed.

A. Negative neon state

If all orbital electrons were retained, a $^{21}Ne^{-}$ state would be formed. A calculation based on a nonrelativistic fixed-core valence-shell configuration interaction predicts the existence of a metastable Ar^{-} state, but the metastable Ne^{-} state is expected to decay to the continuum through an E1 transition[26]. Direct searches found Ar^{-} with a lifetime of ~350 ns, and conclude that if Ne^{-} exists its lifetime is $\ll$ 50 ns[27], in agreement with the calculation. Even if Ne^{-} were metastable with an appreciable lifetime, the probability of remaining negatively charged is small. The calculated negative ion configuration ($1s^2 2s^2 2p^5 3p^2$) is not accessible from the ground state of Na ($1s^2 2s^2 2p^6 3s^1$) because of symmetry. However, due to the 3s↔3p cycling from the trapping lasers, a small portion (~30%) of the population has the configuration $1s^2 2s^2 2p^6 3p^1$. Since the overlap between the Na 2p and Ne 2p state is 97.05%, each 2p electron has less than a 3% chance of being shaken-up to the 3p state. Therefore, the branching ratio for this configuration should be <5.4%. Moreover, with a lifetime $\ll$ 50 ns, $^{21}Ne^{-}$ would be difficult to distinguish from $^{21}Ne^{0}$. We conducted a direct search by reversing the direction of the electric field and found no evidence of $\beta^+-^{21}Ne^{-}$ coincidences or of $\beta^+-^{21}Ne^{0}$ coincidences at shorter than kinematically allowed TOFs. The limits as a function of branching ratio are shown in Fig. 3. We conclude $^{21}Ne^{-}$ should not contribute appreciably to the observed charge state distribution.

B. Neutral neon

The majority of ^{21}Ne daughters are neutral but only 18.5±0.2% reach the MCP active area in coincidence with β^+s with recoil energies of ≤228 eV. The MCP detection efficiency at ~100 eV energies is energy dependent and much smaller than at keV energies. Studies of $^{16}O^{0}$, $^{16}O^{+}$, and $^{16}O^{-}$ with energies between 30–1000 eV indicate detection efficiencies depend on charge state but fall nearly linearly with decreasing energy[28]. Neutrals hit the MCP at angles up to 15°, and MCP gain decreases for angles >5° relative to the microchannel axis[29]. With the 78.1±3.1% $^{21}Ne^{0}$ branching ratio determined here, the MCP detection efficiency is 6.1±0.8%, consistent with results in Ref. [28] for $^{16}O^{0}$.

C. Positive charge states

The relative branching ratios for the positive charge states are determined with fits to a Monte Carlo simula-

TABLE I: Ratio of production of positive ions relative to $^{21}Ne^{+}$ production. Corrections for MCP detection efficiency as well as deadtime losses have been taken into account. The production ratio for ions with charge $\geq$6 is $\leq$0.0003.

Ions Compared	Production Ratio
$^{21}Ne^{+2}/^{21}Ne^{+}$	0.1673±0.0011
$^{21}Ne^{+3}/^{21}Ne^{+}$	0.0143±0.0003
$^{21}Ne^{+4}/^{21}Ne^{+}$	0.0013±0.0003
$^{21}Ne^{+5}/^{21}Ne^{+}$	0.0006±0.0003

tion. Event loss due to more than one β or MCP trigger falling in the same coincident window is included in the analysis. The TOF distribution for $\gamma-^{21}$Ne coincidences is determined from events that trigger the E but not the ΔE detector. A measured value of 1.05±0.23% for the 0.511 keV γ ray Compton scattering probability in the ΔE detector determines its contribution in the fit.

The $^{21}Ne^{+q}$ accelerate to energies of $\sim 9.0\times q$ [keV], and impact at angles of $<2^{\circ}$ at the MCP. Refs. [29–35] conclude that above $\sim$2 keV detection efficiency approaches the MCP open area ratio of $\sim$60%, independent of ion species or charge state. The relative detection efficiency for the positive charge states was determined by estimating the percentage of MCP pulses below the electronic threshold for a given charge state, amounting to a $<$2% correction. The relative charge state distribution is given in Table I.

D. Absolute charge state distribution

The absolute branching ratios are determined from the source strength and detection efficiency for $\beta^{+}-^{21}$Ne coincidences. The branching ratio, Γ_q, is given by

$$\Gamma_q = \frac{R_q}{R_T} \tag{1}$$

where R_q is the detection rate of ion recoils with charge $+q$ and R_T is given by

$$R_T = \frac{N \ln 2}{\tau_{1/2}} \Omega_{MCP} \Omega_\beta \mathcal{E}_{MCP} \mathcal{E}_\beta L. \tag{2}$$

Here N is the average number of ^{21}Na atoms in the trap, $\tau_{1/2}$ the halflife, Ω_{MCP} and Ω_β the detector solid angles, $\mathcal{E}_{MCP}$ and $\mathcal{E}_\beta$ the detection efficiencies, and L the fraction of detector live time. These values and associated uncertainties are shown in Table II. The neutral branching ratio is determined by subtraction. N is estimated from the trap fluorescence, F, by

$$N = \frac{F}{R \Omega_{ph} C} \tag{3}$$

where Ω_{ph} is the PMT solid angle, and C is the efficiency. The intensity of radiated light is

$$R = \frac{\Gamma}{2} \frac{s}{1 + s + \frac{4(2\pi\delta)^2}{\Gamma^2}} \tag{4}$$

TABLE II: Relavent values and uncertainties in the quantities needed for calculating the charge state branching ratios.

Quantity	Value	Uncertainty
N	269,000	29,000
$\tau_{1/2}$[s]	22.48	0.04
Ω_{MCP}	0.996	0.001
Ω_β	0.0092	0.0002
$\mathcal{E}_{MCP}$	0.58	0.05
$\mathcal{E}_\beta$	0.968	0.001
L	0.95	0.01
R_{+1}[Hz]	7.58	0.01
R_T[Hz]	40.9	5.7
Γ_{+1}	0.185	0.026

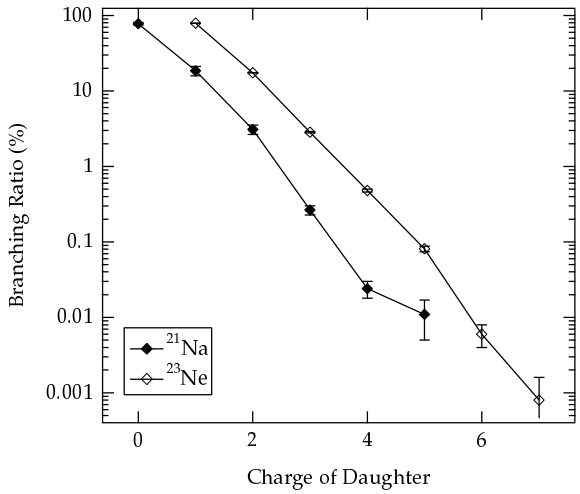

FIG. 4: Comparison of charge state distributions of ^{21}Na and ^{23}Ne. Points are connected to guide the eye.

with saturation parameter, s, natural linewidth, Γ, and detuning of laser light, δ.

E. Comparison with ^{23}Ne β^{-} decay

Fig. 4 shows a comparison of the daughter charge state distribution following ^{21}Na β^{+} decay with the β^{-} decay of ^{23}Ne. One might expect the β^{+} charge state distribution to be similar to the β^{-} distribution shifted by a charge of +2 because of the difference in sign of ΔZ. The branching ratios, however, are remarkably similar when shifted one unit of charge. This implies that an extra electron, most likely the valence electron, is frequently lost in ^{21}Na β^{+} decay, leading to positive ions following 21.9±2.6% of decays instead of $\sim$5%.

F. Dependence of charge state distribution on energy of decay products

In the "sudden approximation", electrons are ejected because of orbital mismatch following the sudden change in nuclear charge by ΔZ, independent of the energy of the emitted β. However, electron shake-off diminishes the β decay phase space[22] and becomes more likely at small β energies. The effect is more pronounced for atoms with large binding energies. In addition, ionization from the β energy dependent direct collision mechanism is predicted to increase with orbital binding energy. Therefore, even though shake-off from deeply bound K shells is small, the energy dependence can be significant.

In neon, 99% of K shell vacancies lead to subsequent Auger transitions[36], so K shell ionization contributes significantly to the production of $^{21}Ne^{+2}$ (~30%) but not $^{21}Ne^{+}$ (<0.1%), in the model discussed below. We do not expect +1 ion production should exhibit significant β energy dependence, although higher charge states may. Although for β decay correlation studies the singly charged ions provide the bulk of the statistics, consistent results for each charge state are required for a conclusive result. The ratio of $^{21}Ne^{+2}$ to $^{21}Ne^{+}$ as a function of β energy is therefore sensitive to energy dependence of ionization of the K shell. The large ratio of Q-value to B_K in ^{21}Na (>2500) ensures that the β decay phase space is minimally impacted. A calculation using non-relativistic hydrogenic wavefunctions for the ^{21}Ne K shell[37] demonstrates even if all ionization resulted from K shell electron loss, the systematic effect for β decay correlations in ^{21}Na would be <0.1%.

The ratio of K shell electrons ejected per decay by direct collisions ($P_K(DC)$) versus shake-off ($P_K(SO)$) for a decay with a mean β kinetic energy of $\overline{E}_\beta$ was first estimated by Feinberg[38] to be

$$\frac{P_K(DC)}{P_K(SO)} \approx \frac{B_K}{\overline{E}_\beta}. \quad (5)$$

However, more recent calculations have shown the DC mechanism in β^+ decays with endpoint energies of ~1 MeV is enhanced by 15–20 times more than this estimate[39, 40]. A comparable enhancement in ^{21}Na would give a contribution to K shell ionization of ~1%.

In β^+ emitters[41–44], P_K has been measured only over an average of the β energy distribution by detecting K shell x-rays in coincidence with annihilation γ-rays to isolate β^+ from EC decays. We measured the energy dependence in the ion charge state yields. Any increase in charge state ratios at low energies in Fig. 5 could be a signature of direct collisions. Assuming the β energy dependence predicted by Feinberg[45], the DC mechanism contributes <1.3% to the production of $^{21}Ne^{+2}$ ions, or <4.2% to the ionization of the K shell, and <4.3% to the production of $^{21}Ne^{+3}$ ions. Calculations indicate that for β decays to the first excited state of ^{21}Ne, internal conversion of the 350 keV γ-ray can safely be neglected as it leads to additional ionization in $\lesssim$0.007% of excited state decays[46]. Approximately 0.9% of the ^{21}Na decays through EC but do not trigger the acquisition.

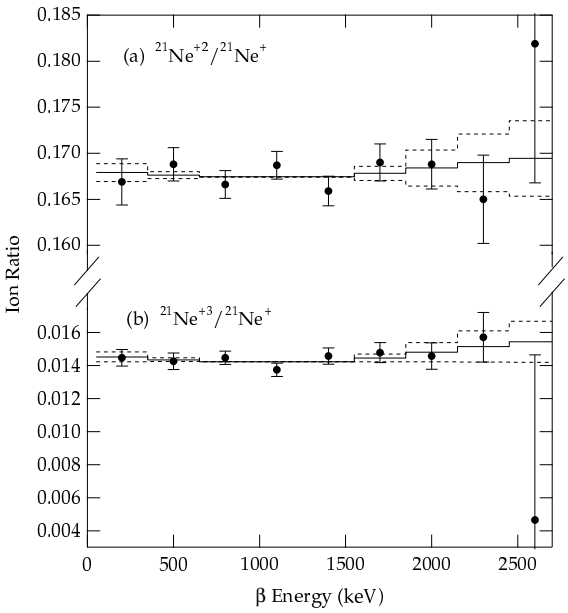

FIG. 5: Ratio of (a) $^{21}Ne^{+2}/^{21}Ne^{+}$ and (b) $^{21}Ne^{+3}/^{21}Ne^{+}$ versus total energy deposited in β detector. Note the scale change between (a) and (b). The energy extends beyond the ^{21}Na endpoint because of interactions between annihilation γ-rays and the scintillator volume. A correction has been applied because the collection efficiency for $^{21}Ne^{+}$ in coincidence with low energy β^+s is slightly less than 100%. A horizontal line would indicate the absence of β and recoil energy influence on ionization. The solid line shows the best fit for recoil ioinization, while the dashed line shows ± 1 σ fits (for a fixed ratio at 1100 keV). The fits yield 2.6±5.4% and 17±18% for recoil ionization in the ion ratios $^{21}Ne^{+2}/^{21}Ne^{+}$ and $^{21}Ne^{+3}/^{21}Ne^{+}$, respectively.

The β^+ energy also gives information about daughter nucleus recoil energy. At intermediate energies the momenta of the β and ν can cancel causing minimal nuclear recoil. The ion ratios in Fig. 5 are consistent with no recoil ionization, with contributions of 2.6±5.4% and 17±18% respectively. Although these are the first published limits for β^+ decay, they are not stringent enough for current precision β decay work or to test the predictions of the calculation described below. For this, recoil ionization needs to be studied at the level of $\lesssim$1%.

V. CALCULATIONS

The expected charge state distribution is calculated using the "sudden approximation" as the nuclear charge changes and the nucleus receives a momentum kick from the decay. The overlap between initial and final state orbitals determines the probability the electron will be found in that final state orbital. Further ionization can occur through Auger transitions and accompanying ad-

TABLE III: Charge state distribution branching ratios (%).

Charge	Including $n=3$	Neglecting $n=3$	^{21}Na
-1	54.59[a]	0.0	0.0
0	35.31	78.3	78.1±3.1
1	7.04	17.8	18.5±2.6
2	2.39	3.06	3.10±0.44
3	0.58	0.660	0.265±0.037
4	0.08	0.135	0.024±0.006
5	0.009	0.0235	0.011±0.006
6	0.002	0.0033	≤0.010
7	≤0.0002	0.0005	≤0.006
8	≤0.0002	≤0.0001	≤0.006

[a]Negative ions would be indistinguishable from neutrals because of their short lifetime.

ditional shake-off.

The probability of finding an electron (originally in orbital ψ_i of nucleus of charge Z) in orbital ψ'_f of charge $Z+\Delta Z$ is

$$P(\psi_i \to \psi'_f) = |\langle\psi_i|e^{-i\vec{k}_r\cdot\vec{x}}|\psi'_f\rangle|^2. \quad (6)$$

In the rest frame of the nucleus of mass M, the electrons (of mass m_e) are imparted a momentum of $|\hbar\vec{k}_r| = m_e\sqrt{\frac{2E_r}{M}}$ from a recoil of energy E_r. Usually $\vec{k}_r\cdot\vec{x}$ is assumed to be sufficiently small so that $e^{-i\vec{k}_r\cdot\vec{x}} \approx 1$. However, expanding to first order in $\vec{k}_r\cdot\vec{x}$ gives

$$P(\psi_i \to \psi'_f) \approx |\langle\psi_i|\psi'_f\rangle|^2 + k_r^2|\langle\psi_i|\vec{k}_r\cdot\vec{x}|\psi'_f\rangle|^2. \quad (7)$$

The first term is due to orbital mismatch and we use it to calculate the charge state distribution. The second term is proportional to the recoil nucleus' energy (and is of order $k_r^2\cdot a_0^2 Z^{\frac{2}{3}} \sim 10^{-3}$ for ^{21}Na) and is used to estimate the magnitude of recoil ionization.

A. Charge state distribution

Single electron wavefunctions for the ground states of Na and Ne have been calculated using the Roothaan-Hartree-Fock expansion technique[47]. Hydrogenic orbitals have been used in estimates of the overlap between the ground state orbitals of Na and 3s and 3p state of Ne. Any electron not retained in a $n \le 3$ shell is assumed to go to an autoionizing state or to the continuum. The Ne atomic configuration is generated from the final state orbital of each electron, limiting each orbital to single occupancy.

Additional electron ejection can result from the rearrangement of the electronic cloud since 1s or 2s orbital vacancies can undergo further ionization by Auger processes and associated shake-off. A number of calculations of these vacancy cascades have been performed[36, 48, 49] with results in reasonable agreement with experiment[50]. At most one electron outside the K and L shells is retained (all others are assumed lost due to Auger transitions). This correction has minimal impact on the results. Combining shake-off and rearrangement ionization determines the charge state distribution. The results are summarized in Table III. The calculation agrees with data only if all electrons outside the K and L shells are ejected. In either case, the production of states with charge ≥3 is overestimated. This is not surprising because the Auger ionization probabilities pertain to a single orbital vacancy and should decrease for a more highly ionized state.

B. Recoil ionization

The second term has the form

$$P_{\rm recoil}(\psi_i \to \psi'_f) = k_r^2|\langle\psi_i|\hat{k}_r\cdot\vec{x}|\psi'_f\rangle|^2$$
$$= \frac{2E_r m_e^2}{\hbar^2 M}|\sum_n \langle\psi_i|\psi'_n\rangle\langle\psi'_n|\hat{k}_r\cdot\vec{x}|\psi'_f\rangle|^2. \quad (8)$$

Making the approximation $\langle\psi_i|\psi'_n\rangle \approx \delta_{in}$ we find

$$P_{\rm recoil}(E_r) \approx \frac{3m_e}{M}\left(\int_{I_P}^{\infty}\frac{df_{osc}}{dE_{if}}E_{if}^{-1}dE_{if}\right)E_r$$
$$= P_{\rm recoil}(E_r^{max})\frac{E_r}{E_r^{max}} \quad (9)$$

where $\frac{df_{osc}}{dE_{if}}$ is the differential oscillator strength, E_{if} the energy difference between initial and final states, I_P the ionization potential, and E_r^{max} the maximum recoil energy. For orbital electrons with small binding energies, and therefore small momenta, the perturbation is greatest. The percent increase, I_q, in the production of charge state q for the highest energy recoils compared to zero energy recoils is

$$I_q = 100\times P_{\rm recoil}(E_r^{max})\frac{(\Gamma_{q-1}-\Gamma_q)}{\Gamma_q} \quad (10)$$

where Γ_q is the branching ratio to ions of charge q.

The accuracy of the calculation can be tested against the measured recoil ionization for ^{6}He. Using measured oscillator strengths for Li^+ transitions[51], we calculate $I_{+1} = 0.38\%$. This crude calculation achieves ∼60% of the experimentally determined value of 0.63±0.10%[3]. The effect is so large because of the large nuclear velocities resulting from a decay with a large E_0 and small M.

For ^{21}Na we calculate $I_{+1} \approx 0.6\%$, using measured oscillator strengths for neutral Ne transitions to the continuum[52] and the measured charge state branching ratios. In general this effect is ∼4 times larger for +1 ions from β^+ decay compared to β^- decay of identical E_0 and M because of smaller branching ratios to positive ions and lower daughter binding energies. Although inconsequential to the charge state distribution, it is a

TABLE IV: Percent increase in production of +1 ions between highest and lowest energy recoils, I_{+1}, for various β^+ emitters currently being trapped.

Isotope	E_r^{max}(eV)	I_{+1}(%)
^{21}Na	228	0.6
^{38m}K	424	3.1
^{37}K	455	3.4
^{82}Rb	98	1.3
^{78}Rb	103	1.5
^{80}Rb	140	1.9

potentially large systematic effect for β decay correlation experiments currently attaining the 0.01 level and seeking to reach precision of 0.001. An I_{+1} of 1% would lead to a systematic error of $\sim$0.005 in the $\beta - \nu$ correlation coefficient, a. The results of this calculation for the β^+ unstable nuclei ^{21}Na, ^{38m}K[10], ^{37}K[10], ^{82}Rb[53], and ^{78}Rb[10], (using experimentally determined Ar and Kr oscillator strengths[54]), each of which are currently being trapped for precision β decay studies, are shown in Table IV. For the case of one and two electron systems, precise calculations of recoil induced ionization have been performed[20] but no such calculations exist for systems with $\geq$3 electrons. More detailed calculations or precise measurements of recoil ionization will be necessary to interpret the results of future β decay correlation experiments.

VI. CONCLUSION

Measurement of the charge state distribution in ^{21}Na shows that $\sim$20% of the decays shake-off $\geq$2 electrons, leading to positive ions, compared with only $\sim$5% of β^- decays in which 2 or more electrons are lost. This is fortuitous for experiments that manipulate the positive daughter ions for detection. At the current level of precision obtained by these experiments ($\sim$0.01 for the $\beta - \nu$ correlation), the independence of the charge state distribution from the energies of the β and recoil ion are sufficient. However, a rough calculation indicates that the influence of the nuclear recoil on the ionization process cannot be ignored for measurements of β correlations using β^+ emitters surpassing the level of $\sim$1% and needs to be studied further. For β^- emitters, however, the effect is smaller since all decays result in positive ions. For β^+ decays that yield stable negative ions, such as ^{19}Ne[55], the impact of recoil ionization is uncertain because of the competing effects of a large branching ratio to negative ions and small orbital binding energies. The β energy dependence of ionization is small ($\lesssim$1%) as expected in ^{21}Na but could be significant for decays with low Q-values or high Z.

Acknowledgments

We appreciate the assistance of the technical staff at the 88-Inch Cyclotron. This work was supported by the Director, Office of Energy Research, Office of Basic Energy Sciences, of the U.S. Department of Energy under Contract No. DE-AC03-76SF00098.

[1] J. S. Allen et al., Phys. Rev. **116**, 134 (1959).
[2] B. W. Ridley, Nucl. Phys. **25**, 483 (1961).
[3] C. H. Johnson, F. Pleasonton, and T. A. Carlson, Phys. Rev. **132**, 1149 (1963).
[4] T. A. Carlson, Phys. Rev. **132**, 2239 (1963).
[5] W. P. Alford and D. R. Hamilton, Phys. Rev. **105**, 673 (1957).
[6] M. M. Hindi et al., Phys. Rev. C **58**, 2512 (1998).
[7] I. don't know yet, to be published.
[8] P. Delahaye et al., Hyperfine Interactions **132**, 479 (2001).
[9] D. Beck et al., Nucl. Phys. A **701**, 369 (2002).
[10] A. Gorelov et al., Hyperfine Interactions **127**, 373 (2000).
[11] T. A. Carlson, F. Pleasonton, and C. H. Johnson, Phys. Rev. **129**, 2220 (1963).
[12] T. A. Carlson, Phys. Rev. **130**, 2361 (1963).
[13] A. H. Snell and F. Pleasonton, Phys. Rev. **107**, 740 (1957).
[14] T. A. Carlson, Phys. Rev. **131**, 676 (1963).
[15] A. H. Snell and F. Pleasonton, Phys. Rev. **100**, 1396 (1955).
[16] O. Kofoed-Hansen, Phys. Rev. **96**, 1045 (1954).
[17] F. Pleasonton and A. H. Snell, Proc. Roy. Soc. (London) A **241**, 141 (1957).
[18] A. H. Snell and F. Pleasonton, Phys. Rev. **111**, 1338 (1958).
[19] A. H. Snell, F. Pleasonton, and J. L. Need, Phys. Rev. **116**, 1548 (1959).
[20] L. Wauters et al., J. Phys. B **30**, 4569 (1997).
[21] T. Mukoyama and S. Ito, Phys. Lett. A **131**, 182 (1988).
[22] P. Stephas and B. Crasemann, Phys. Rev. **164**, 1509 (1967).
[23] Y. Isozumi, T. Mukoyama, and S. Shimizu, Phys. Rev. Lett. **29**, 298 (1972).
[24] Z.-T. Lu et al., Phys. Rev. Lett. **72**, 3791 (1994).
[25] M. Rowe et al., Phys. Rev. **59**, 1869 (1999).
[26] C. F. Bunge, M. Galan, R. Jauregui, and A. V. Bunge, NIM **202**, 299 (1982).
[27] Y. K. Bae, J. R. Peterson, A. S. Schlachter, and J. W. Stearns, Phys. Rev. Lett. **54**, 789 (1985).
[28] T. M. Stephen and B. L. Peko, Rev. Sci. Instrum. **71**, 1355 (2000).

[29] R. S. Gao et al., Rev. Sci. Instrum. **55**, 1756 (1984).
[30] T. Sakurai and T. Hashizume, Rev. Sci. Instrum. **57**, 236 (1986).
[31] A. Muller, N. Djuric, G. H. Dunn, and D. S. Belic, Rev. Sci. Instrum. **57**, 349 (1986).
[32] A. Bader et al., Meas. Sci. Technol. **6**, 959 (1995).
[33] B. Brehm, J. Grosser, T. Ruscheinski, and M. Zimmer, Meas. Sci. Technol. **6**, 953 (1995).
[34] J. Oberheide, P. Wilhelms, and M. Zimmer, Meas. Sci. Technol. **8**, 351 (1997).
[35] H. C. Straub et al., Rev. Sci. Instrum. **70**, 4238 (1999).
[36] A. G. Kochur, V. L. Sukorukov, A. I. Dudenko, and P. V. Demekhin, J. Phys. B **28**, 387 (1995).
[37] J. S. Levinger, Phys. Rev. **90**, 11 (1953).
[38] E. L. Feinberg, J. Phys. (USSR) **4**, 423 (1941).
[39] R. L. Intemann, Phys. Rev. A **28**, 1288 (1983).
[40] I. S. Batkin, K. A. Bushahma, T. A. Churakova, and S. L. Demakov, J. Phys. G **18**, 1995 (1992).
[41] S. K. Nha, G. Schupp, and H. J. Nagy, Phys. Rev. C **27**, 1276 (1985).
[42] R. D. Scott, J. Phys. G **9**, 303 (1983).
[43] R. D. Scott, J. Phys. G **6**, 1427 (1980).
[44] G. Schupp and M. S. Freedman, Phys. Rev. C **21**, 348 (1980).
[45] E. L. Feinberg, Soviet J. of Nucl. Phys. **1**, 438 (1965).
[46] I. M. Band, M. B. Trzhaskovskaya, and M. A. Listengarten, At. Data and Nucl. Data Tables **18**, 433 (1976).
[47] E. Clementi and C. Roetti, At. Data and Nucl. Data Tables **14**, 177 (1974).
[48] G. Omar and Y. Hahn, Z. Phys. D **25**, 31 (1992).
[49] A. El-Shemi, Y. Lofty, and G. Zschornack, J. Phys. B **30**, 237 (1997).
[50] T. A. Carlson, W. E. Hunt, and M. O. . Krause, Phys. Rev. **151**, 41 (1966).
[51] E. Hollauer and M. A. C. Nascimento, Phys. Rev. A **42**, 6608 (1990).
[52] W. F. Chan, G. Cooper, X. Guo, and C. E. Brion, Phys. Rev. A **45**, 1420 (1992).
[53] S. G. Crane et al., Phys. Rev. Lett. **86**, 2967 (2001).
[54] W. F. Chan et al., Phys. Rev. A **46**, 149 (1992).
[55] D. R. Maxson, J. S. Allen, and W. K. Jentschke, Phys. Rev. **97**, 109 (1955).